A&A 365, 347–359 (2001)
DOI: 10.1051/0004-6361:20000045

Astronomy & Astrophysics

Evolution of photoionization and star formation in starbursts and H II galaxies

E. Moy[1], B. Rocca-Volmerange[1,2], and M. Fioc[1,3]

[1] Institut d'Astrophysique de Paris, 98bis boulevard Arago, 75014 Paris, France
[2] Institut d'Astrophysique Spatiale, Bât. 121, Université Paris XI, 91405 Orsay Cedex, France
[3] NASA/Goddard Space Flight Center, code 685, Greenbelt, MD 20771, USA

Received 17 January 2000 / Accepted 4 September 2000

Abstract. We analyze coherently the stellar and nebular energy distributions of starbursts and H II galaxies, using our evolutionary synthesis model, PÉGASE (Fioc & Rocca-Volmerange 1997, 2000), coupled to the photoionization code CLOUDY (Ferland 1996). The originality of this study is to relate the evolution and the metallicity of the starburst to the past star formation history of the host galaxy. Extinction and geometrical effects on emission lines and continua are computed in coherency with metallicity. We compare our model predictions to an observed sample of ≈750 H II regions and starbursts. When fitting $[\mathrm{O\,III}]_{\lambda4363}/[\mathrm{O\,III}]_{\lambda5007}$, $[\mathrm{O\,I}]_{\lambda6300}/\mathrm{H}\alpha$, $[\mathrm{S\,II}]_{\lambda\lambda6716,6731}/\mathrm{H}\alpha$, $[\mathrm{N\,II}]_{\lambda6584}/\mathrm{H}\alpha$ and $[\mathrm{O\,III}]_{\lambda5007}/\mathrm{H}\beta$, the most striking feature is the decreasing spread in U with increasing metallicity Z. High-U objects systematically have a low metallicity while low levels of excitation happen at any Z. The best fits of emission line ratios are obtained with a combination of a high- and a low-ionization components. No additional source of ionizing photons – shocks or hidden AGN – is needed. The high level of excitation observed in metal-poor H II galaxies requires a very young population (≤ 3 Myr), while starburst nuclear galaxies (SBNGs) are consistent with a wider range of age (≤ 5 Myr). Colors ($B-V$, $V-R$) and equivalent widths are fitted in coherency with emission line ratios. An underlying population is needed, even for small-aperture observations. This underlying population not only reddens the continuum and dilutes the equivalent width of the emission lines, but also participates in the ionization process. Its main effect on line ratios is to maintain a high level of excitation when the burst stops. Models combining underlying populations typical of Hubble sequence galaxies and instantaneous starbursts with ages between 0 and 8 Myr agree satisfactorily with all the data.

Key words. galaxies: starburst – galaxies: evolution – galaxies: stellar content – ISM: H II regions

1. Introduction

The "starburst" phenomenon calls to mind a class of objects dominated by the radiation of massive stars (Gallego et al. 1995) embedded in a dusty H II region. Modelling starbursts consistently is the key to interpret the properties of the actively star-forming galaxies detected at a redshift $z > 2$ (Giavalisco et al. 1996; Madau et al. 1996; Steidel et al. 1996; Lowenthal et al. 1997). To this purpose, the extensive study of local samples is a requisite step.

Local starbursts span a wide range of types, from individual H II regions in spiral arms to blue compact H II galaxies and huge kpc-scale nuclear starbursts (Coziol et al. 1998). Types differ from one another in their main characteristics (line ratios, equivalent widths, colors), and presumably have different stellar populations and physical conditions. So, is it possible to find correlations between the basic properties: age, initial mass function, metallicity, relative distributions of stars, gas and dust? Among these, which one dominates spectral properties? In which range do parameters vary? Answering these questions requires a consistent model of starbursts coupling the evolution of stars, dust and gas.

The first studies dealing with emission lines of H II regions (Shields 1974, 1978; Stasińska 1978, 1980; McCall et al. 1985) relied on single-star photoionization models. Average physical properties of large starburst samples were deduced from these pioneering works. As an example, a relation between the metallicity Z and the ionization parameter U was derived by Dopita & Evans (1986) by fitting the emission line ratios from large samples of extragalactic H II regions.

More realistic stellar populations of star clusters were computed by McGaugh (1991) with the Salpeter (1955) initial mass function (IMF), to calibrate metallicity dependant line ratios. Further improvements were the implementation of theoretical tracks of massive stars, allowing to follow the evolution in time of a starburst (e.g. García-Vargas & Díaz 1994). Thanks to the computation of

Send offprint requests to: E. Moy, e-mail: moy@iap.fr

Table 1. Data sources. SBNG: starburst nucleus galaxies; H IIG: H II galaxies; H II: H II regions

References	Starburst type	Balmer absorption correction	Reddening correction
Terlevich et al. 1991	H IIG, SBNG	no	no
Veilleux & Osterbrock 1987	SBNG	no	no
Veilleux et al. 1995	IRAS SBNG	yes	no
French 1980	H IIG	no	no
Leech et al. 1989	IRAS SBG	yes	yes
Storchi-Bergmann et al. 1995	H IIG, SBNG	no	no
Contini et al. 1998	IRAS SBNG, H II	yes	no

evolutionary tracks for various metal abundances, the influence of the metallicity could also be studied (Cid-Fernandes et al. 1992; Cerviño & Mas-Hesse 1994; Olofsson 1997; García-Vargas et al. 1995a,b; Stasińska & Leitherer 1996). Evans (1991) emphasized the importance of using up-to-date stellar atmosphere models to calibrate nebular diagnostics. The most recent models take into account modern, updated stellar physics (Leitherer & Heckman 1995; Leitherer et al. 1999), in particular the impact on stellar spectra of line blanketing and of departures from local thermodynamic equilibrium (Stasińska & Schaerer 1997).

Till now, only a few large datasets covering a wide range of physical conditions have been analyzed with state-of-the-art models, coupling evolving stellar populations and photoionization. Stasińska & Leitherer (1996), for example, restricted their analysis to metal-poor ($Z < Z_{\odot}/4$) objects. As a matter of fact, statistical properties of starbursts are not definitely established. A metal-dependent IMF was early proposed as an explanation for the $[\mathrm{O\,III}]_{\lambda5007}/\mathrm{H}\beta$ decrease at high Z (Terlevich 1985; Shields & Tinsley 1976). Although a standard IMF seems in agreement with the bulk of observations (Leitherer 1998), the IMF slope (see e.g. Eisenhauer et al. 1998; Greggio et al. 1998) and mass cut-offs (Goldader et al. 1997) are still under debate.

Our aim is hereafter to study the evolution of the spectral properties of aging starbursts with the help of models taking into account the effects of metallicity, geometry, dust and the excitation level of the gas. To avoid normalization problems, we selected relative properties independent of distance (colors, equivalent widths and line ratios). We focused on emission line ratios at close wavelengths – thus reducing reddening effects – to study the ionizing spectrum and the excitation of the gas. Equivalent widths and colors are used preferentially to study age effects, as well as the impact of the spatial distribution of stars, gas and dust.

The observational sample is presented in Sect. 2. The coupling of the codes PÉGASE, to model the evolution of star formation and stellar emission, and CLOUDY, for a consequent photoionization of the gas by massive stars in a given geometry, is described in Sect. 3. The relation between the metallicity Z and the ionization parameter U is analyzed in Sect. 4, while equivalent widths and colors are considered in Sect. 5. The contribution of an underlying population is analyzed in Sect. 6. Discussion and conclusion are respectively in Sects. 7 and 8.

2. A selected sample of starbursts and H II galaxies

Our data set (Table 1) is a selection of 754 objects from observational samples of galaxies having properties characteristic of starbursts: intense emission lines (French 1980; Veilleux & Osterbrock 1987; Terlevich et al. 1991), strong far-infrared emission (Leech et al. 1989; Veilleux et al. 1995), or excess of blue or ultraviolet emission (Storchi-Bergmann et al. 1995); in addition, Contini et al. (1998) require galaxies to have a bar. Objects dominated by an active galactic nucleus (AGN) are excluded from our sample, though some of them may be faintly contaminated by nuclear activity. Effects of aperture and differences in data reduction processes are considered in Sect. 2.2.

2.1. Spectral classification of the original sample

Objects listed in the source papers are classified in two families. The first one includes metal-poor H II galaxies (H IIGs) and extra-nuclear H II regions, both likely devoid of active nucleus. The second one gathers galactic central regions where the ionized-gas emission could be partly due to shocks (Kim et al. 1998) or AGNs (see Heckman 1991 and references therein). To select only starburst nucleus galaxies (SBNGs) in this last class, we keep the classification of the authors, which is based on the pioneering works of Baldwin et al. (1981, hereafter BPT) and Veilleux & Osterbrock (1987, hereafter VO).

The Terlevich et al. (1991) sample is mainly composed of H IIGs with some possible SBNGs. The authors used two of the BPT criteria based on the $[\mathrm{O\,III}]_{\lambda5007}/\mathrm{H}\beta$ and $[\mathrm{O\,II}]_{\lambda3727}/[\mathrm{O\,III}]_{\lambda5007}$ ratios. We also analyzed their sample with the VO method and obtained the same classification.

Contini et al. (1998) adopted the VO criteria. Their sample includes SBNGs and giant H II regions located in IRAS barred spiral galaxies, selected from Mazzarella & Balzano (1986) and listed in the Lyon-Meudon Extragalactic Database (LEDA).

Table 2. Comparison with predictions of coupled models available in the literature. Top: García-Vargas et al. 1995); age = 1 Myr, $Z = Z_\odot$, $\log(U) = -3.11$. Bottom: Stasińska & Leitherer (1996); age = 1 Myr, $Z = Z_\odot$, $\log(U) = -2.60$

Line	PÉGASE+CLOUDY	García-Vargas et al. (1995)
$\log(\mathrm{H}\beta)$ [erg s^{-1}]	38.83	38.84
$[\mathrm{O\,II}]_{\lambda3727}/\mathrm{H}\beta$	3.10	3.07
$[\mathrm{O\,III}]_{\lambda5007}/\mathrm{H}\beta$	0.31	0.25
$[\mathrm{O\,I}]_{\lambda6300}/\mathrm{H}\beta$	0.04	0.04
$[\mathrm{N\,II}]_{\lambda6584}/\mathrm{H}\beta$	1.34	1.34
$[\mathrm{S\,II}]_{\lambda6716}/\mathrm{H}\beta$	0.57	0.58
$[\mathrm{S\,II}]_{\lambda6731}/\mathrm{H}\beta$	0.39	0.40
$[\mathrm{S\,III}]_{\lambda9069}/\mathrm{H}\beta$	0.36	0.34

Line	PÉGASE+CLOUDY	Stasińska & Leitherer (1996)
$\log(\mathrm{H}\beta)$ [erg s^{-1}]	40.56	40.56
$[\mathrm{O\,II}]_{\lambda3727}/\mathrm{H}\beta$	$2.57\ 10^{-1}$	$2.75\ 10^{-1}$
$[\mathrm{O\,III}]_{\lambda5007}/\mathrm{H}\beta$	$8.18\ 10^{-1}$	$7.37\ 10^{-1}$
$[\mathrm{O\,I}]_{\lambda6300}/\mathrm{H}\beta$	$2.60\ 10^{-3}$	$3.13\ 10^{-3}$

Two samples contain only SBNGs located inside IRAS galaxies. Veilleux et al. (1995) followed both BPT and VO criteria, while Leech et al. (1989) used only some of the criteria of BPT. Actually, an important part of their sample lies far beyond the limit reported by VO between H II-like regions and AGNs in the $[\mathrm{O\,III}]/\mathrm{H}\beta$ vs. $[\mathrm{O\,I}]/\mathrm{H}\alpha$ and $[\mathrm{O\,III}]/\mathrm{H}\beta$ vs. $[\mathrm{N\,II}]/\mathrm{H}\alpha$ diagrams. These objects are clearly misclassified and have been excluded from our selection. Storchi-Bergmann et al. (1995) reported observations of emission line galaxies of various types. Following Coziol et al. (1998), all compact galaxies are hereafter classified as H II galaxies, whether dwarf or not. Finally, we include in our selection the observations of five starbursts from the sample of Balzano (1983) reported by VO, and the data of French (1980) on 14 H IIGs.

2.2. Homogeneity of reddening, aperture and absorption corrections

Most line ratios considered here are computed from close lines; so, reddening effects should be small and will be neglected in the following.

In most samples, the contamination, through large apertures, of the starburst light by the host galaxy population is likely to increase the continuum emission and to dilute the equivalent width of emission lines. To avoid this problem, we will restrict the analysis of colors and equivalent widths to the sample of Contini et al. (1998). These data were acquired with a long-slit spectrograph, but the spectra presented by the authors correspond to Hα emitting regions exclusively. Hence, the contamination of the starburst continuum by the environment of the host galaxy should be very weak.

The host galaxy can also modify the apparent line ratios involving Balmer lines through the presence of stellar absorption lines. Emission line fluxes are corrected for this effect as follows:

$$F_{\mathrm{line}}^{\mathrm{corr}} = F_{\mathrm{line}}^{\mathrm{obs}} \left(1 + \frac{W_{\mathrm{line}}^{\mathrm{abs}}}{W_{\mathrm{line}}^{\mathrm{obs}}}\right), \quad (1)$$

where $F_{\mathrm{line}}^{\mathrm{corr}}$ and $F_{\mathrm{line}}^{\mathrm{obs}}$ are respectively the absorption-corrected and the apparent emission line fluxes, and $W_{\mathrm{line}}^{\mathrm{abs}}$ and $W_{\mathrm{line}}^{\mathrm{obs}}$ are the absorption and measured emission equivalent widths. Not all the samples were corrected (Table 1). The correction should be negligible for the Hα line because $W_{\mathrm{H}\alpha}^{\mathrm{abs}} \ll W_{\mathrm{H}\alpha}^{\mathrm{obs}}$. It is stronger for H$\beta$ (up to 100% in Leech et al. 1989) and the ratio $[\mathrm{O\,III}]/\mathrm{H}\beta$ may be affected. This ratio is systematically higher in the samples of French (1980) and Terlevich et al. (1991), mainly composed of H IIGs, than in the other ones, which include mainly SBNGs. Is this trend real, or is it due to the fact that these two data sets are not corrected for underlying stellar lines? Note that Storchi-Bergmann et al. (1995) already noticed that $[\mathrm{O\,III}]/\mathrm{H}\beta$ is higher in H II galaxies than in SBNGs. Moreover, the correction for absorption lines should be very small in H IIGs, since these objects have simultaneously large $W_{\mathrm{H}\beta}^{\mathrm{obs}}$ (67 Å in Terlevich et al. 1991) and low $W_{\mathrm{H}\beta}^{\mathrm{abs}}$. Hence, we conclude that the trend we observe is real and not due to the discrepancies between the reduction procedures.

3. The coupling of spectral evolution and photoionization

The evolutionary synthesis code we use, PÉGASE, takes into account metallicity and dust effects. PÉGASE computes the stellar spectral energy distributions (SEDs) and the metallicities of starbursts and galaxies of the Hubble sequence at any stage of evolution, within the metallicity range $Z = 10^{-4}$ to 10^{-1}. Typical parameters of PÉGASE are the star formation rate (SFR) and the initial mass

Table 3. Adopted solar abundances and prescriptions for abundance variations with Z

Element X	$(X/H)_{Z_\odot}$	$(X/H)_Z$
He	0.107	$0.08096 + 0.01833 \times Z/(0.7\ Z_\odot)$
B	$2.63\ 10^{-11}$	$(\mathrm{B/H})_{Z_\odot} \times Z/Z_\odot$
C	$3.63\ 10^{-4}$	$(\mathrm{C/H})_{Z_\odot} \times Z/Z_\odot$
O	$8.51\ 10^{-4}$	$(\mathrm{O/H})_{Z_\odot} \times Z/Z_\odot$
F	$3.63\ 10^{-8}$	$(\mathrm{F/H})_{Z_\odot} \times Z/Z_\odot$
Na	$2.14\ 10^{-6}$	$(\mathrm{Na/H})_{Z_\odot} \times Z/Z_\odot$
P	$2.82\ 10^{-7}$	$(\mathrm{P/H})_{Z_\odot} \times Z/Z_\odot$
Cl	$3.16\ 10^{-7}$	$(\mathrm{Cl/H})_{Z_\odot} \times Z/Z_\odot$
Ar	$3.63\ 10^{-6}$	$(\mathrm{Ar/H})_{Z_\odot} \times Z/Z_\odot$
Fe	$4.86\ 10^{-5}$	$(\mathrm{Fe/H})_{Z_\odot} \times Z/Z_\odot$

log(N/O)
$12.43 - 3.77(\log(\mathrm{O/H}) + 12) + 0.26(\log(\mathrm{O/H}) + 12)^2$

function. The new version[1] used hereafter, PÉGASE.2, is based on the evolutionary tracks of Girardi et al. (1996), Fagotto et al. (1994a–c) and Bressan et al. (1993). The AGB to post-AGB phases are computed following the prescriptions of Groenewegen & de Jong (1993) models. The synthetic stellar spectral library is from Kurucz (1992), modified by Lejeune et al. (1997) to fit observed colors. For details, see Fioc & Rocca-Volmerange (1999, 2000, in preparation).

The photoionization code CLOUDY (version 90.04, Ferland 1996) predicts the spectra of low- to high-density astrophysical plasmas in the most extreme astrophysical sites, such as starbursts and quasar environments. It takes into account recent changes in atomic databases and new numerical methods. In addition to its physical performances, the code was chosen for its easy Web access, its documentation and its friendly on-line help. CLOUDY proposes options to explore the influence of geometrical factors: type of geometry – spherical or plane parallel –, covering factor $\Omega/(4\pi)$, filling factor f, and the distance R from the source to the plasma.

The coupling of PÉGASE.2 with CLOUDY allows to compute coherently the stellar and nebular emission, and to fit simultaneously the continuum and lines from stellar populations embedded in a gas cloud. The metallicity $Z(t)$, and the stellar SED – in particular the energy distribution of the ionizing photons – provided by PÉGASE are used as inputs by CLOUDY. Hereafter, we call Q_{H^0} the emission rate of ionizing photons. This quantity is used to normalize the SEDs computed by PÉGASE.

The results of the current version of the code have been compared to those obtained by similar "coupled models". They are presented in Table 2 for two sets of predictions: the model 16 from García-Vargas et al. (1995b), and the $Z_\odot$-model computed by Stasińska & Leitherer (1996) for a $10^6\,M_\odot$-cluster. In both cases, we used inputs matching the reference model (IMF, age, geometrical parameters and chemical abundances). For the first comparison test, the agreement is very good (Table 2, top). Our results also agree relatively well with those of Stasińska & Leitherer (1996), given that the evolutionary tracks, the spectral libraries and the photoionization codes are different in the two models.

[1] This code is available at `http://www.iap.fr/users/fioc/PEGASE.html` or by anonymous ftp at `ftp.iap.fr` in `/pub/from_users/pegase`

3.1. Star formation parameters

An instantaneous star formation episode ("pure starburst") is assumed for starbursts – a scenario well suited to study emission line properties. In Sect. 6, we will also consider an underlying stellar population formed either during a previous burst or continuously. We tentatively tested several IMFs of the form $\mathrm{d}N/\mathrm{d}m \propto m^{-\alpha}$, $m \in [M_{\mathrm{low}}, M_{\mathrm{up}}]$: $\alpha = -2.35$, $m \in [0.1, 120]\,M_\odot$ (Salpeter 1955); $\alpha = -3.35$, $m \in [0.1, 120]\,M_\odot$; and $\alpha = -2.35$, $m \in [3, 30]\,M_\odot$. The last one is truncated, as suggested by various infrared studies (Rieke et al. 1993; Lançon & Rocca-Volmerange 1996). The initial metallicity is left as a free parameter.

3.2. Physical properties of the gas

The emission line spectrum of an ionized nebula depends on the combination of the ionizing spectrum, the chemical composition of the gas and the so-called ionization parameter U.

The elemental abundances of the gas have been made consistent with the metallicity of the ionizing stars. The solar abundances used here are given in Table 3. All the abundances were scaled linearly according to the metallicity, except for nitrogen and helium. For the likely secondary element N, we adopted the law proposed by Coziol et al. (1999), multiplied by a factor 1.5 to account for the excess of nitrogen observed in starbursts. For He, we

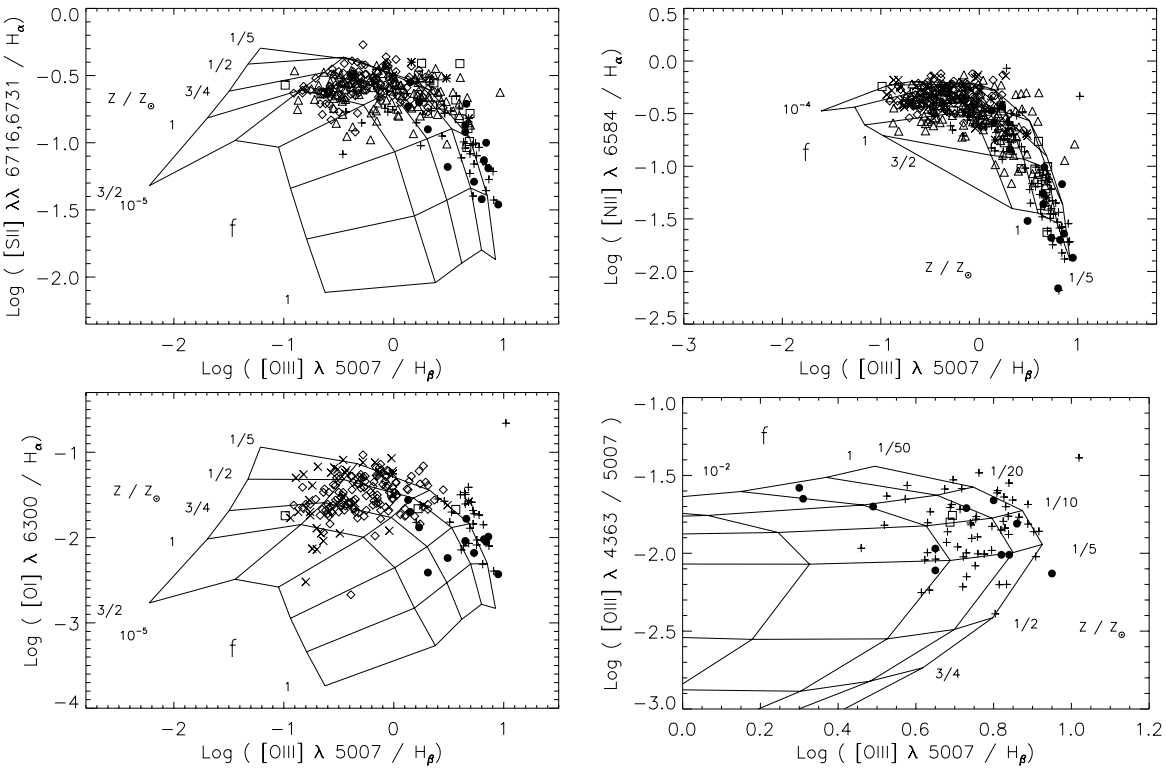

Fig. 1. Models of pure instantaneous starbursts for various filling factors (f) and metallicities (Z). The data are from Terlevich et al. ("plus" signs), Veilleux & Osterbrock (asterisks), French (filled circles), Veilleux et al. (diamonds), Contini et al. (triangles), Storchi-Bergmann et al. (squares) and Leech et al. (crosses)

followed a prescription proposed by Dopita & Kewley (private communication; see Table 3 for details).

The ionization parameter U is defined as:

$$U = \frac{Q_{\mathrm{H}^0}}{4\pi R_{\mathrm{s}}^2 n_{\mathrm{H}} c}, \tag{2}$$

where n_{H} is the hydrogen density, c the speed of light, and R_{s} the Strömgren radius (i.e. the radius of the ionization front). Taking into account the inner radius R (e.g. Evans & Dopita 1985), R_{s} is roughly equal to:

$$R_{\mathrm{s}} = \left(\frac{3Q_{\mathrm{H}^0}}{4\pi\alpha_{\mathrm{B}} n_{\mathrm{H}}^2 f} + R^3 \right)^{1/3}, \tag{3}$$

where α_{B} is the case B temperature-dependent recombination coefficient and f is the filling factor. This formula highlights the impact of each parameter on U, but is only approximate, since it assumes a constant temperature through all the nebula. The effective Strömgren radius is obtained only at the end of a CLOUDY calculation.

The spherical geometry (Stasińska & Leitherer 1996; González-Delgado et al. 1999) and plane-parallel geometry (García-Vargas & Díaz 1994; García-Vargas et al. 1997) are extreme situations for which the right-hand side of Eq. (3) is respectively dominated by the first and the second term. The adopted geometry was spherical. The hydrogen density n_{H} was 100 cm^{-3} in most models, but we also computed a few cases for $n_{\mathrm{H}} = 10$ and $n_{\mathrm{H}} = 1000$ cm^{-3}, to assess the specific impact of density on emission line ratios. We set the number of ionizing photons to $Q_{\mathrm{H}^0} = 10^{52}$ photons s^{-1}, corresponding to a maximum luminosity of $\sim 10^{40}$ erg s^{-1} in the Hα emission line – a value characteristic of intense star formation sites (Shields 1990). For emission lines, the exact value of Q_{H^0} is not important as long as the density does not exceed the critical limit of collisional de-excitation, below which models with the same U, ionizing spectrum and metallicity predict the same line ratios. To obtain reasonable values for U, we varied the volume filling factor between 10^{-5} and 1 and set R to 4 pc.

We assume that the gas is distributed in a spherical shell covering a solid angle Ω around the star cluster. The covering factor $\Omega/(4\pi)$ was allowed to vary in the interval [0.1, 1]. The continuum luminosity from the starburst F_λ (erg s^{-1} Å^{-1}) at any wavelength λ is:

$$F_\lambda = F_\lambda^{\mathrm{trans}} + F_\lambda^{\mathrm{neb}} + F_\lambda^{\mathrm{stell}}. \tag{4}$$

The transmitted stellar continuum $F_\lambda^{\mathrm{trans}}$ and the nebular continuum F_λ^{neb} both scale with $\Omega/(4\pi)$. $F_\lambda^{\mathrm{stell}}$, scaling as $(1 - \Omega/(4\pi))$, refers to the part of the stellar spectrum not crossing the gas (and thus not contributing to the ionization process).

3.3. Extinction of the spectrum

Assuming a dust screen at the outer edge of the H II region, the continuum flux is reddened as follows:

$$F_\lambda = (F_\lambda^{\mathrm{trans}} + F_\lambda^{\mathrm{neb}}) \mathrm{e}^{-\tau_\lambda^{\mathrm{neb}}} + F_\lambda^{\mathrm{stell}}\ \mathrm{e}^{-\tau_\lambda^{\mathrm{stell}}}. \tag{5}$$

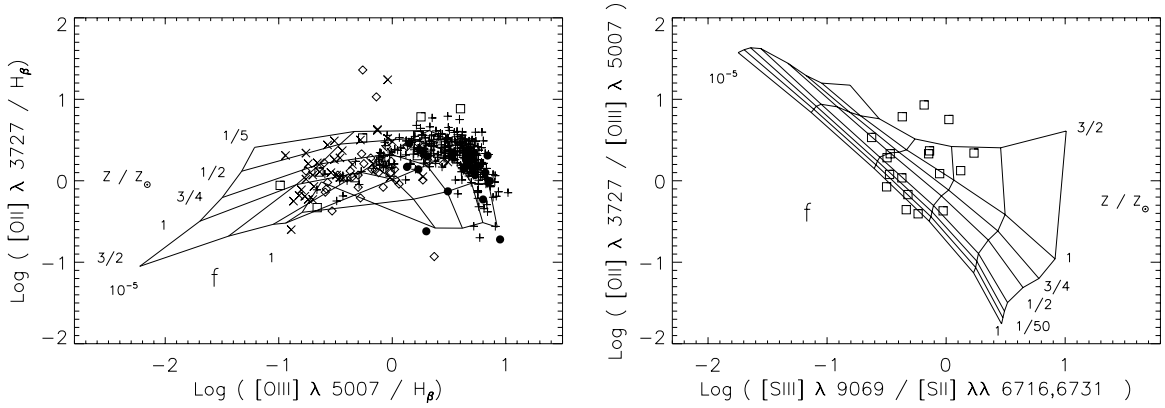

Fig. 2. Same as Fig. 1 for line ratios sensitive to reddening

Emission line fluxes are also multiplied by $e^{-\tau_\lambda^{neb}}$. The optical depth τ_V^{neb} was a free parameter, as well as the $\tau_V^{stell}/\tau_V^{neb}$ ratio (≤ 1). This option takes into account a possible dust concentration outside the nebula rather than on the line-of-sight not covered by the gas. The variation of the optical depth with wavelength is derived from the metallicity-dependent extinction laws of the Magellanic Clouds and our Galaxy.

4. Results on emission line ratios for instantaneous starburst models

We have explored the impact of the IMF, the age of the starburst, the metallicity and the ionization parameter on the following optical line ratios: $[O\,III]_{\lambda4363}/[O\,III]_{\lambda5007}$, $[O\,I]_{\lambda6300}/H\alpha$, $[S\,II]_{\lambda\lambda6716,6731}/H\alpha$, $[N\,II]_{\lambda6584}/H\alpha$ and $[O\,III]_{\lambda5007}/H\beta$. The value of f was varied between 10^{-5} and 1. The corresponding $\log(U)$ (as defined in Sect. 3.2) belongs to $[-5.5, -1.5]$. Note that similar results could also be derived by varying the inner radius R (in a plane-parallel geometry), the density n_H or a combination of both.

In the following, if not specified, the IMF is Salpeter (1955).

4.1. Metallicity effects

Emission line ratios are sensitive to the metallicity through two competing effects. On the one hand, the opacity increases with Z, lowering the stellar effective temperatures and thus the hardness of the ionizing spectrum. A trend towards lower excitation levels is therefore expected in high-Z starbursts, even if there is no dependence of the IMF or the geometry on the metallicity. This effect is reinforced at high Z by the efficient cooling by metals and thus the low electronic temperature T_e.

On the other hand, the energy in metal emission lines tends naturally to increase with higher elemental abundances. For oxygen lines, this process dominates at $Z \leq 1/5\,Z_\odot$, while the opposite happens at higher metallicity (e.g. McGaugh 1991). As a consequence, two models with metallicities respectively below and above this limit can predict comparable emission lines. For this reason, we present hereafter our predictions for Z in the range $[1/50, 3/2]\,Z_\odot$ if no degeneracy happens in the considered diagram, but in $[1/5, 3/2]\,Z_\odot$ otherwise.

4.2. Effects of the geometrical filling factor f

For a given density n_H, varying the filling factor f changes the optical depth per unit length and the ionization structure: the smaller f, the smaller the mean ionization level, and the lower the luminosities of high excitation lines such as $[O\,III]_{\lambda5007}$. Low-excitation lines behave inversely.

Models of pure instantaneous starbursts, with metallicities in the range $[1/5, 3/2]\,Z_\odot$, are compared to the data in Fig. 1 for six values of the filling factor f: 10^{-5}, 10^{-4}, 10^{-3}, 10^{-2}, 10^{-1}, and 1. The data are largely covered by the models when at least two parameters vary – here chemical and geometrical. Interestingly, different types of objects seem to occupy different zones in the $Z-U$ plane: H II galaxies are in better agreement with low-Z (1/50 $Z_\odot$ to 3/4 $Z_\odot$), high-U models ($f \in [10^{-3}, 1]$); SBNGs are compatible with low values of f (10^{-5} to 10^{-2}), but encompass a wide range of metallicities.

We also report in Fig. 2 the comparison of predictions with observations in following diagrams: $[O\,II]_{\lambda3727}/H\beta$ vs. $[O\,III]_{\lambda5007}/H\beta$ and $[O\,II]_{\lambda3727}/[O\,III]_{\lambda5007}$ vs. $[S\,III]_{\lambda9069}/[S\,II]_{\lambda\lambda6716,6731}$. Note that the $[O\,II]/H\beta$, $[O\,II]/[O\,III]$ and $[S\,III]/[S\,II]$ ratios are sensitive to reddening and, for this reason, we do not include them in the discussion. We can only notice that, given the uncertain impact of dust on these ratios, our results are compatible with the observations.

4.3. The apparent relation between Z and U: Degeneracy problems

A mean $U-Z$ relation fitting the data could easily be derived from Fig. 1, as in Dopita & Evans (1986). However, this relation would suffer from too many uncertainties: first, it would not take into account the high Z-low Z degeneracy; second, age effects are very similar to

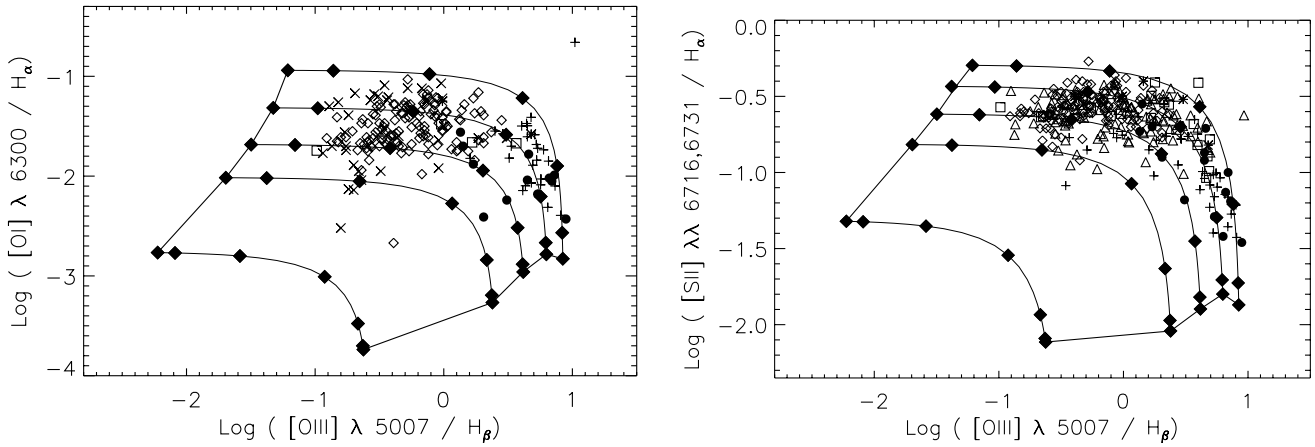

Fig. 3. Comparison of the data with five sequences obtained by varying the relative weights of the high ($f = 1$) and low ($f = 10^{-5}$) excitation components. Solid diamonds are the points for which the low excitation component contributes to 0, 1, 10, 50, 90, 99 and 100% of the Hβ flux (from right to left)

Table 4. Variations of line ratios induced by a change of density. The age is 0 Myr and the metallicity is $Z_\odot/5$

$n_{\rm H}$	f	$\log(U)$	[O III]$_{\lambda5007}$/Hβ	[O I]$_{\lambda6300}$/Hα	[S II]$_{\lambda\lambda6716,6731}$/H$\alpha$
10 cm^{-3}	1	−1.89	7.53	2.74 10^{-3}	2.39 10^{-2}
	10^{-1}	−2.57	5.88	8.47 10^{-3}	6.77 10^{-2}
	10^{-2}	−3.24	3.35	2.27 10^{-2}	1.69 10^{-1}
	10^{-3}	−3.92	1.04	5.13 10^{-2}	3.29 10^{-1}
	10^{-4}	−4.61	0.17	9.17 10^{-2}	3.29 10^{-1}
1000 cm^{-3}	1	−1.29	9.29	8.88 10^{-4}	7.11 10^{-3}
	10^{-1}	−1.91	8.27	2.90 10^{-3}	2.08 10^{-2}
	10^{-2}	−2.57	6.47	8.90 10^{-3}	5.93 10^{-2}
	10^{-3}	−3.25	3.66	2.39 10^{-2}	1.49 10^{-1}
	10^{-4}	-3.92	1.12	5.44 10^{-2}	2.93 10^{-1}

those induced by the metallicity. This is illustrated in Fig. 4, where [O I]/Hα and [S II]/Hα vs. [O III]$_{\lambda5007}$/Hβ are plotted for $Z_\odot/5$ at $t = 0$, 4, 5 and 6 Myr. Variations of the IMF give rise to similar uncertainties, as shown in Fig. 6: the lower number of massive stars for a steeper or truncated IMF causes a strong decrease of both [O III]/Hβ and [O I]/Hα, just as if the metallicity was higher.

Due to this age-metallicity-IMF degeneracy, a meaningful $Z-U$ analytical relation cannot be established on the basis of line ratio diagrams. Moreover, Fig. 1 clearly shows that the *dispersion* of U, rather than the mean value of this parameter, is linked to the metallicity: while starbursts exist at any U at low Z, only low-U starbursts are observed at high metallicity. We consider a possible cause of this trend in the next paragraph.

4.4. The upper envelope of the data sequences

In the [O I]/Hα vs. [O III]/Hβ and [S II]/Hα vs. [O III]/Hβ diagrams, many data points lie above predictions, even when the misclassified objects of Leech et al. (1989) are excluded from the sample. To check whether this discrepancy can be solved by varying the density, we have performed two series of calculations at $Z = Z_\odot/5$ with $n_{\rm H} = 10$ and 1000 cm^{-3}. We chose this metallicity because the corresponding sequence defines the upper envelope of our model grid in these diagrams. The results are shown in Table 4. The main one is that model sequences with different densities largely overlap: clearly, the outliers cannot be explained by a variation of $n_{\rm H}$.

Many authors have proposed that a faint contribution from shocks or AGNs could explain the intensity of the [O I] line in starbursts (see e.g. Stasińska & Leitherer 1996). We consider here an alternative possibility where there are, inside the starburst, both high- and low-excitation zones, due for example to a distribution of gas and stars more complex than the classical geometry adopted in our calculations. To test this hypothesis, we computed a series of sequences obtained by varying the relative weight of high- and low-excitation models ($f = 1$ and $f = 10^{-5}$, respectively) for five metallicities. The results (Fig. 3) are in much better agreement with the data than pure U sequences, as they explain both the trend and the dispersion of the observations. Another advantage

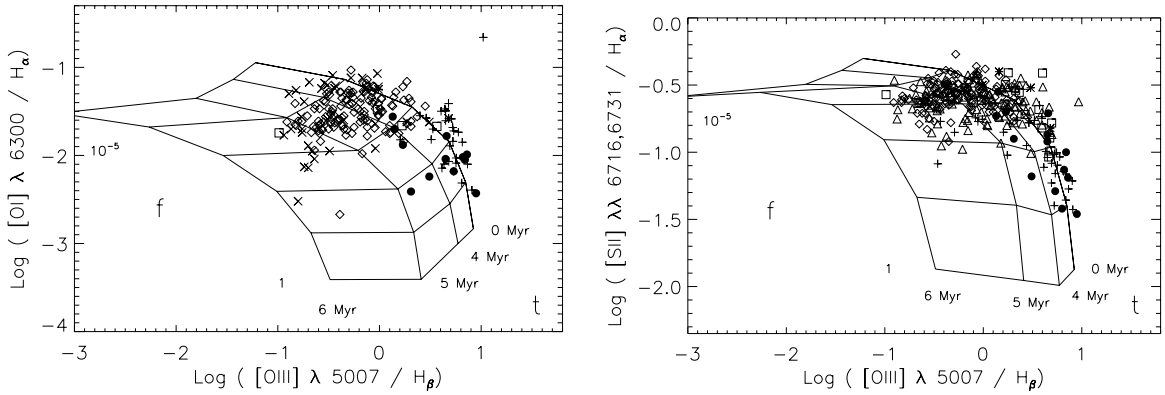

Fig. 4. Evolution with the starburst age of the $Z_\odot/5$-model sequence plotted in Fig. 1

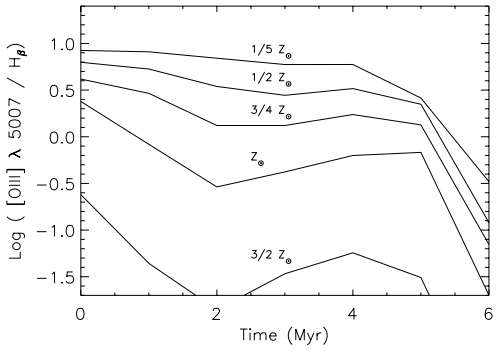

Fig. 5. Time evolution of the $[\mathrm{O\,III}]_{\lambda5007}/\mathrm{H}\beta$ ratio for instantaneous starbursts. The decrease of the ratio after 5 Myr is very rapid and puts severe constraints on the age of starbursts (see text for details)

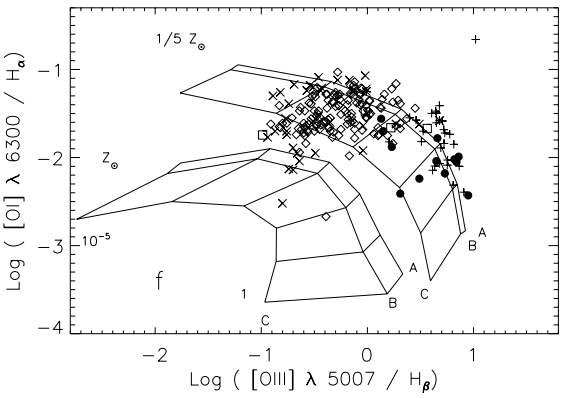

Fig. 6. Impact of the IMF on $[\mathrm{O\,I}]/\mathrm{H}\alpha$ vs. $[\mathrm{O\,III}]/\mathrm{H}\beta$ for two metallicities ($Z_\odot/5$ and $Z_\odot$). In each case, three f sequences are plotted: A ($\alpha = -2.35$, $M_{\rm low} = 0.1\,M_\odot$ and $M_{\rm up} = 120\,M_\odot$), B ($\alpha = -3.35$, $M_{\rm low} = 0.1\,M_\odot$ and $M_{\rm up} = 120\,M_\odot$) and C ($\alpha = -2.35$, $M_{\rm low} = 3\,M_\odot$ and $M_{\rm up} = 30\,M_\odot$)

of this explanation is that no other source of ionization, such as AGNs or shocks, is required. If this hypothesis is correct, the evolution of the apparent U with Z in fact corresponds to the presence in low-metallicity objects of a high-U component, which is absent in high-Z starbursts. We come back to this point in the discussion.

4.5. Constraints on age and IMF

Figure 5 shows the evolution, up to 6 Myr, of the $[\mathrm{O\,III}]_{\lambda5007}/\mathrm{H}\beta$ ratio for the models plotted in Figs. 1 and 2. The constraints on age shown by this plot are very strong, though noticeably different for H II galaxies and SBNGs: H II galaxies, of high-excitation level, need the high energy photons emitted by massive stars, so that only young ($\leq$3 Myr) models are compatible with observations (see Sect. 7); SBNGs, requiring a lower excitation level, span a wider range of ages. In any case, the rapid drop of the $[\mathrm{O\,III}]/\mathrm{H}\beta$ ratio after 5 Myr requires the presence of stars younger than 6 Myr.

Line ratios depend on the hardness of the spectrum, and so on the IMF. The [O I] line, emitted from the partly ionized zone, requires high-energy photons and is thus particularly sensitive to the high-mass end of the IMF. Figure 6 presents the sensitivity of $[\mathrm{O\,I}]_{\lambda6300}/\mathrm{H}\alpha$ and $[\mathrm{O\,III}]/\mathrm{H}\beta$ to the initial mass function. A Salpeter IMF is favored by our results, in good agreement with recent studies (e.g. Stasińska & Leitherer 1996; García-Vargas et al. 1995). An interesting point is that the steeper and truncated IMFs, while clearly excluded by the data for high-U H IIGs, are acceptable for metal-rich starbursts.

5. Results on equivalent widths and colors: covering factor and extinction

In the following, we aim to keep our previous fits of emission line ratios and, simultaneously, to reproduce $W(\mathrm{H}\alpha)$ and $B-V$ and $V-R$ colors from the sample of Contini et al. (1998). The models plotted in Figs. 1 and 2 predict Hα equivalent widths above 500 Å, while the observed $W(\mathrm{H}\alpha)$ seldom exceed 300 Å. Predicted equivalent widths in excess to the observations are a well-known problem (Bresolin et al. 1999 and references therein). The hypothesis of a "density bounded" nebula (Leitherer et al. 1996) is ruled out by the observed intensities of the low-ionization lines; the reduction of the thickness of the partly-ionized zone would lead to lower $[\mathrm{S\,II}]/\mathrm{H}\alpha$ and $[\mathrm{O\,I}]/\mathrm{H}\alpha$ than in Fig. 1, and the models would not fit any more these line ratios.

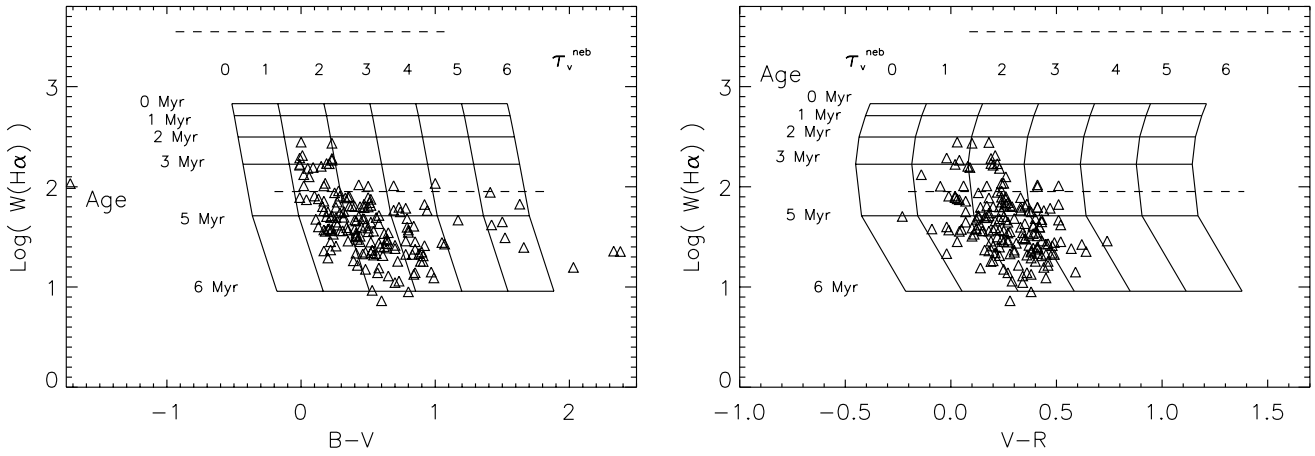

Fig. 7. Pure starburst models for various ages (0 to 6 Myr) and τ_V between 0 to 6. The ratio $\tau_V^{\rm stell}/\tau_V^{\rm neb} = 0.5$ is equal to 1. The covering factor is 0.1. Data (triangles) are from Contini et al. (1998). The solid lines indicate the predictions of the $\Omega/(4\pi) = 0.1$ model grid. The two dashed lines show the $t = 0$ Myr (upper line) and $t = 6$ Myr (lower line) model results for $\Omega/(4\pi) = 1$

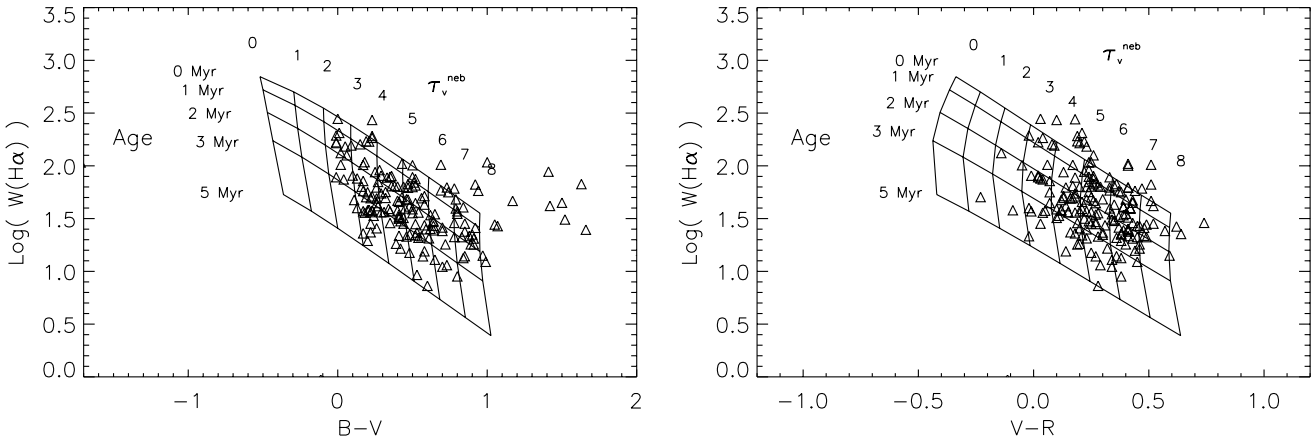

Fig. 8. Same as Fig. 7, but for $\tau_V^{\rm stell}/\tau_V^{\rm neb} = 0.5$ (see Sects. 3.3 and 5)

A low covering factor $\Omega/(4\pi)$ reduces the equivalent widths by increasing the stellar emission relative to the nebular one, *without changing line ratios*. A similar explanation of the faint $W(\mathrm{H}\beta)$ of blue compact and irregular galaxies was suggested by Mas-Hesse & Kunth (1999).

Figure 7 shows the influence of dust and age in the $W(\mathrm{H}\alpha)$ vs. $B-V$ and $W(\mathrm{H}\alpha)$ vs. $V-R$ planes, for $\Omega/(4\pi) = 0.1$. For comparison, we also show $t = 0$ and $t = 6$ Myr sequences for $\Omega/(4\pi) = 1$. We plot only $Z = Z_\odot$ models, since the metallicity has only weak effects on $B-V$, $V-R$ and $W(\mathrm{H}\alpha)$. Similarly, for such a low value of $\Omega/(4\pi)$, f hardly affects the colors and the only models in Fig. 7 are for $f = 1$. Ages between 0 and 6 Myr, $\tau_V^{\rm stell}/\tau_V^{\rm gas} = 1$ and $\tau_V^{\rm gas}$ in the range [0,6] are suggested by the $W(\mathrm{H}\alpha)$ vs. $B-V$ diagram. However, $\tau_V \geq 4$ is excluded by the $V-R$ data, and ages ≥ 6 Myr are incompatible with line ratios (see also Sect. 7.2).

A ratio $\tau_\lambda^{\rm stell}/\tau_\lambda^{\rm gas} \simeq 0.5$ (following Calzetti et al. 1997; see also Fanelli et al. 1988; Keel 1993; Mas-Hesse & Kunth 1999) can simultaneously fit $B-V$ and $V-R$, but requires very high extinctions, up to $\tau_V^{\rm neb} = 8$ (Fig. 8), while Contini et al. (1998) derived a maximum value of $\sim$4 from the Balmer decrement. The $B-V$ of the reddest objects are considered as anomalous (Contini, private communication) and are not reproduced by any model.

6. The contribution of an evolved population

The distribution of the data in the $W(\mathrm{H}\alpha)$ vs. $B-V$ or $V-R$ diagrams is very difficult to explain with pure instantaneous starburst models. The main problem is the very low covering factor required. An alternative hypothesis, able to explain the equivalent widths and colors of the Contini et al. (1998) sample with the much more reasonable value $\Omega/(4\pi) = 0.5$, is the presence of evolved stars inside the starburst. Such a population, created during past formation episodes, can account for the observed weakness of equivalent widths by increasing the continuum (e.g. McCall et al. 1985; Díaz et al. 1991). It may also explain the red colors of the sample without requiring huge amounts of dust.

We considered two possible underlying populations. The first one consists of an instantaneous burst which

Table 5. Parameter values of starburst + host scenarios. (a): Host galaxy age (in Myr) when starburst occurs. (b): star formation parameter ν (in Myr^{-1}) of the host galaxy. (c) Time-scale of gas infall onto the host galaxy (Myr). (d): fraction of ionizing photons emitted by the host population when the starburst starts in models A, B, C, D and E (see text)

$Z/Z_\odot$	$t_{\rm gal}$ (a)	$\nu\ 10^{-3}$ (b)	$t_{\rm c}$ (c)	% (host) (d) A	B	C	D	E
1/5	11 000	0.02	5000	100.0	21.0	11.7	2.5	0.0
1/2	11 000	0.05	5000	100.0	17.9	9.6	2.5	0.0
3/4	13 000	0.05	2000	100.0	16.2	8.9	1.9	0.0
1	13 000	0.1	2000	100.0	14.5	7.8	1.9	0.0
3/2	13 000	0.15	2000	100.0	12.4	6.6	1.7	0.0

occured 100 Myr ago. This old burst is assumed to have been ten times more intense than the current one. The predictions of these models are plotted in Fig. 9. As in Fig. 8, $\tau_\lambda^{\rm stell}/\tau_\lambda^{\rm neb}$ is set to 0.5. However, these models face two problems: first, it is still necessary to extend the age of the young burst to $t = 6$ Myr, unless the covering factor is much lower than the value adopted in Fig. 9 (0.5); second, the sum of the evolved and the young population does not reproduce the colors. To reconcile this type of models with the data, it would be necessary to assume that the old burst was systematically ∼100 times more intense than the current one.

The second type of underlying population is assumed to have formed continuously. We computed a series of scenarios matching the observations of standard Hubble sequence galaxies at $z = 0$, and added a starburst. For the sake of consistency, the initial metallicity of the burst is the current metallicity $Z(t)$ of the host galaxy and is provided by PÉGASE.

The input parameters are chosen so that the starburst metallicities belong to the range $[1/5\,Z_\odot, 3/2\,Z_\odot]$ derived from line ratios. Each scenario is defined by three parameters: the age $t_{\rm gal}$ of the host galaxy when the starburst occurs; the infall timescale $t_{\rm c}$ used to parameterize the accretion rate of the galaxy; the gas-to-star conversion efficiency, ν, relating the star formation rate $\zeta(t)$ to the gas density $\sigma(t)$ by the Schmidt law $\zeta(t) = \nu\sigma(t)$.

Five models (A, B, C, D, E) were computed for each scenario, corresponding to five different contributions of the evolved population to the total emission: A is the pure host galaxy, E is the pure starburst and B, C and D are intermediate cases. Note that the star formation does not stop after the burst, but returns to the quiescent regime. The fraction of ionizing photons due to the underlying population immediately after the burst is given in Table 5, as well as the values of $t_{\rm gal}$, $t_{\rm c}$, and ν for the considered scenario.

Figure 10 presents the impact of the parameters on colors and equivalent widths. We compare the results of model D at $Z = Z_\odot/2$ to the sample of Contini et al. (1998). We also show the results of model C for $Z = 1/2\,Z_\odot$, and the predictions of model D for $3/2\,Z_\odot$. The filling factors are 10^{-2} at $1/2\,Z_\odot$ and $5\ 10^{-4}$ at $3/2\,Z_\odot$. As in Fig. 8, $\tau_\lambda^{\rm stell}/\tau_\lambda^{\rm neb}$ is set to 0.5. However, the covering factor (0.5) is significantly higher, and the $\tau_V^{\rm neb}$ range (0 to 4) is much more reasonable.

Another important point is that, contrary to the pure starburst case, ages of 6 Myr and more are compatible with emission line ratios. This is due to the presence of massive stars, formed after the burst in the underlying population. The presence of such stars ensures that the line ratios are virtually unchanged compared to their values during the burst. Contrary to the case of a burst that occured 100 Myr ago, these scenarios are able to explain simultaneously the colors, the equivalent widths and the line ratios in our sample. They do not require very high levels of extinction, and, maybe more important, do not imply a covering factor lower than 0.5. For all these reasons, the hypothesis of an underlying population formed continuously is our preferred one.

7. Discussion

7.1. A physical link between the ionization parameter and the metallicity?

Dopita & Evans (1986) proposed an analytical relation between the metallicity and the ionization parameter to describe the observational distribution of line ratios in their sample of extragalactic H II regions. In Sect. 4.3, we saw that such a relation suffers from many degeneracies due to age, IMF and metallicity. Moreover, it seems that the quantities which are really related are the dispersion of U and the metallicity.

What could be the physical link between Z and U? According to one hypothesis, this is a link through geometrical effects. Following Castor et al. (1975) and assuming their equations are valid also for a star cluster, the inner radius R of a gaseous shell surrounding a massive star or cluster is:

$$R \propto \left(\frac{\dot{E}t^3}{\rho}\right)^{1/5}, \qquad (6)$$

where $\dot{E}$ is the energy deposition rate of a star (or cluster) of age t in the interstellar medium (ISM) of density ρ.

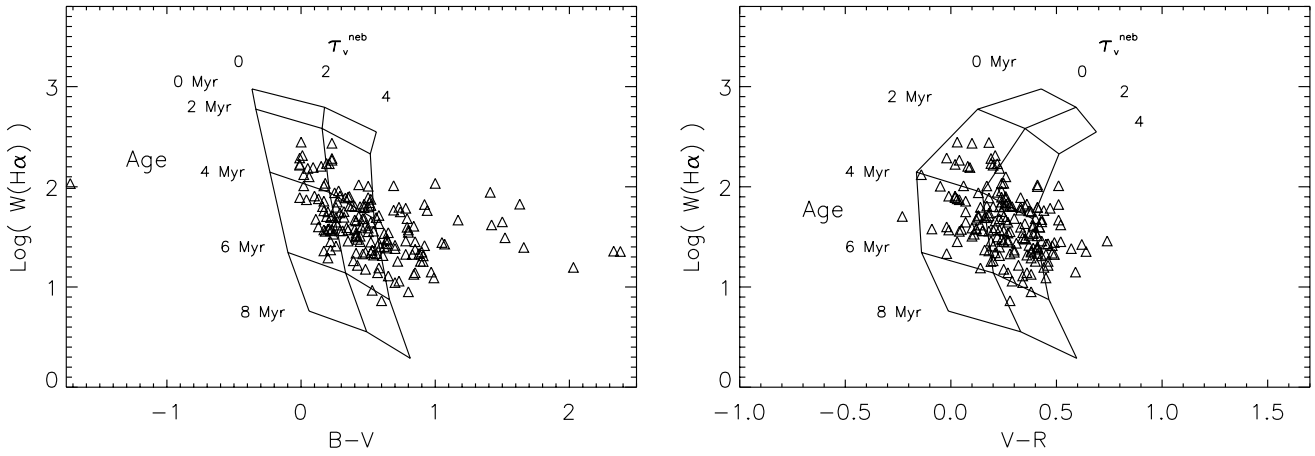

Fig. 9. Hα equivalent widths and colors for instantaneous + 100 Myr-old starbursts. The metallicity of the young starburst is solar. The old burst is assumed to have been ten times more intense than the current one. The model sequences are labeled in terms of the age of the present starburst and of the value of $\tau_V^{\rm neb}$

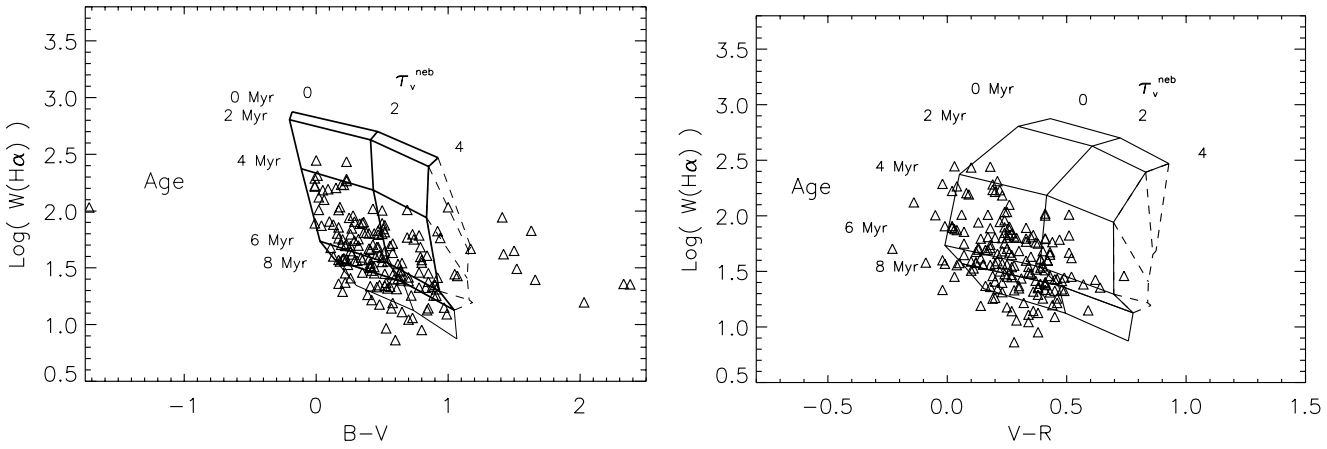

Fig. 10. Hα equivalent widths and colors for instantaneous burst + continuous star formation scenarios. The thick solid lines show the predictions of model D for different ages and extinction levels of the burst. The metallicity of the burst is 1/2 $Z_\odot$. The dashed lines indicate the shift of the right part of the grid when the contribution of the underlying population is increased (model C). The thin solid lines show the shift of the low part of the grid when the metallicity is equal to 3/2 $Z_\odot$

Leitherer et al. (1992) found that $\dot{E}$ is constant for an instantaneous burst until ∼6 Myr and scales linearly with Z, regardless of the age. Hence, high-Z H II regions expand faster.

We therefore propose the following scenario to explain the distribution of starbursts in the line ratio diagrams. For some reason, a site of intense star formation appears in a galaxy with a metal-poor interstellar medium. This starburst can be composed of many individual H II regions surrounding star clusters. As these sub-components evolve with age, the H II regions expand because of stellar winds. At the same time, the enrichment of the ISM by massive-star ejecta begins. If star formation goes on, very young components will coexist inside the starburst with more evolved components. The former will dominate the nebular emission during the first few Myr, and the latter after.

Two additional effects can explain the lack of high-Z and high-U objects: first, at high metallicity, individual H II regions expand faster, leading to a lower ionization parameter; second, according to this scenario, the bulk of nebular emission in high-Z starbursts is produced by evolved, low-excitation H II regions. Checking the validity of this hypothesis requires to model also the expansion of nebulae. This is the subject of a forthcoming paper.

7.2. The equivalent-width problem

The problems encountered by pure starburst scenarios to account for the weakness of the Hα equivalent widths from the sample of Contini et al. (1998) are several. The main one is that a very low covering factor is required. From Figs. 7 and 8, we deduce that a value $\Omega/(4\pi) \sim 0.1$ is necessary to reproduce both W(Hα) and the line ratios in the case of a pure starburst. This means that 90% of the Lyman continuum photons do not contribute to ionization, but are directly absorbed by dust or escape from the starburst. This is in contradiction with many previous studies using Hα or Hβ luminosities to estimate the mass of stellar clusters inside starbursts. In many cases, the agreement between such estimations and those based on

ultraviolet continuum luminosities is excellent (González-Delgado et al. 1999). Some discrepancies appear frequently (Leitherer et al. 1996; Vacca et al. 1995), but they are however weak enough to exclude an absorption fraction of the ionizing photons by the gas as low as 10%. Moreover, observations of diffuse Hα emission in nearby galaxies lead to an estimation of 15–50% for the fraction of ionizing photons escaping from individual H II regions (Kennicutt 1998 and references therein).

Such a systematic low value of the covering factor is therefore clearly ruled out by the observations. Note also that pure starbursts models, even with $\Omega/(4\pi) = 0.1$, cannot reproduce simultaneously the emission line ratios and the equivalent widths (see Sect. 5). Hence, the presence of an evolved stellar population coexisting with a starburst, as analysed in Sect. 6, seems mandatory to explain equivalent widths and colors, even for the data of Contini et al. (1998), who strictly limitated their apertures to Hα-emitting areas. A similar conclusion for galaxies observed through 5-arcsec apertures was drawn by Lançon & Rocca-Volmerange (1996) from the near-infrared spectral synthesis of starbursts.

7.3. Nature of the underlying population

Including underlying populations in the models allows to fit the data in a satisfactory way in the $W(\mathrm{H}\alpha)$ vs. $B-V$ and $V-R$ diagrams with $\Omega/(4\pi) = 0.5$, which means that ∼50% of the ionizing photons escape from the gaseous nebula. This value is close to the 60% fraction suggested by Mas-Hesse & Kunth (1999). The nature of this population remains however elusive.

We have tested an old (100 Myr old) instantaneous burst as a possible underlying population. The agreement with the data, at first sight, is relatively good (Fig. 9). In this case, however, the age of the youngest burst has to extend up to 8 Myr to explain the faint end of the $W(\mathrm{H}\alpha)$ observational distribution. At this age, our models are incompatible with line ratio data. Note that there is no Wolf-Rayet(W-R) star SED in our spectral library; instead, the spectra of the hottest stars available in the library are used during W-R stages. The implementation of W-R SEDs in the library could in principle extend the range of ages compatible with line ratios up to 6 Myr or more. As an example, González-Delgado et al. (1998) obtained an age between 6 and 9 Myr for IRAS 0833+6517. However, this conclusion is based on models with an IMF truncated at $M_{\mathrm{up}} = 30\,M_{\odot}$. Such a low value is clearly excluded for the bulk of our sample (Fig. 6). Moreover, the role of W-R stars in starburst nebular emission is still under debate. According to the most recent studies, the bulk of nebular emission is due to stellar populations younger than 3 Myr (Bresolin et al. 1999).

We have assumed that the old burst was only ten times more intense than the current one. Changing this value to one hundred, for example, would move the predictions in Fig. 9 toward the bottom-right and might explain the bulk of the data with ages lower than, or equal to, 4 Myr. In this case, however, such a difference between past and present star formation remains to be explained.

In this context, the models plotted in Fig. 10 appear as the most attractive ones. Scenarios with an underlying population providing from 2.5 up to 20% of the number of ionizing photons are in acceptable agreement with the data and explain naturally all the observables (emission lines, colors and equivalent widths). The range of τ_V is consistent with the Balmer decrement measurements of Contini et al. (1998). Moreover, the age and metallicity of the underlying population are typically those of normal spirals, suggesting that starbursts are normal events in galaxy evolution. These scenarios draw a coherent picture of the starburst phenomenon, and for this reason, remain the most plausible ones.

8. Conclusion

We have analyzed the emission line and continuum properties of a large sample of starbursts and put new constraints on their stellar populations, metallicity, photoionization state and dust content. Our tool was the spectral evolution code PÉGASE coupled to the photoionization code CLOUDY.

From the comparison of a dataset of emission lines with pure instantaneous starburst scenarios, we have been able to constrain the evolution of the ionization parameter U with the metallicity Z. At high abundance, the high-excitation component clearly detected at low Z is absent or very weak. A preliminary analysis based on energy deposition rate considerations is unsufficient to explain this trend, and a more refined analysis of the dependency of the H II region expansion with Z is needed.

The second important result concerns underlying populations inside starbursts; they are detected even through small-aperture observations. This contribution is needed to reproduce simultaneously all the observables of our sample (line ratios, colors and equivalent widths). The underlying populations are simulated through the whole computation of the past star formation history of the galaxy hosting the starburst. In the scenarios favored by our analysis, the burst itself is supposed to be a brief, intense episode, preceded and followed by a quiescent regime. After the burst, this quiescent formation rate is sufficient to keep the line ratios compatible with the data.

Future prospects should consider the problem of metal depletion on dust grains, since depletion changes the composition of nebular gas. However, the question of the presence of dust *inside* H II regions will be solved only with more constraining data, e.g. those of the ISO satellite. Finally, the large grids computed with the help of a coupled photoionization and stellar evolutionary synthesis model will be also used to study other samples with better statistics.

Acknowledgements. We are pleased to thank Gary Ferland for his multiple consultation and help for the interface with

CLOUDY. M. F. acknowledges support from the National Research Council through the Resident Research Associateship Program.

References

Baldwin, J. A., Phillips, M. M., & Terlevich, R. 1981, PASP, 93, 5 (BPT)

Balzano, V. A. 1983, ApJ, 268, 602

Bresolin, F., Kennicutt, R. C., & Garnett, D. R. 1999, ApJ, 510, 104

Bressan, A., Fagotto, F, Bertelli, G., & Chiosi, C. 1993, A&AS, 100, 647

Calzetti, D., Meurer, G. R., Bohlin, R. C., et al. 1997, AJ, 114, 1834

Castor, J., McCray, R., & Weaver, R. 1975, ApJ, 200, L107

Cerviño, M., & Mas-Hesse, J. M. 1994, A&A, 284, 749

Cid-Fernandes, R., Dottori, H. A., Gruenwald, R. B., & Viegas, S. M. 1992, MNRAS, 255, 165

Contini, T., Considère, S., & Davoust, E. 1998, A&AS, 130, 285

Coziol, R., Carlos Reyes, R.E., Considère, S., Davoust, E., & Contini, T. 1999, A&A, 345, 733

Coziol, R., Torres, C. A. O., Quast, G. R., Contini, T., & Davoust, E. 1998, ApJS, 119, 239

Díaz, A. I., Terlevich, E., Vílchez, J. M., Pagel, B. E. J., & Edmunds, M. G. 1991, MNRAS, 253, 245

Dopita, M. A., & Evans, I. N. 1986, ApJ, 307, 431

Eisenhauer, F., Quirrenbach, A., Zinnecker, H., & Genzel, R. 1998, ApJ, 498, 278

Evans, I. N. 1991, ApJS, 76, 985

Evans, I. N., & Dopita, M. A. 1985, ApJS, 58, 125

Fanelli, M. N., O'Connell, R. W., & Thuan, T. X. 1988, ApJ, 334, 665

Fagotto, F., Bressan, A., Bertelli, G., & Chiosi, C. 1994a, A&AS, 104, 365

Fagotto, F., Bressan, A., Bertelli, G., & Chiosi, C. 1994b, A&AS, 105, 29

Fagotto, F., Bressan, A., Bertelli, G., & Chiosi, C. 1994c, A&AS, 105, 39

Ferland, G. J. 1996, HAZY, a brief introduction to Cloudy, University of Kentucky, Department of Physics and Astronomy Internal Report

Fioc, M., & Rocca-Volmerange, B. 1997, A&A, 326, 950

Fioc, M., & Rocca-Volmerange, B. 2000 [astro-ph/9912179]

French, H. B. 1980, ApJ, 240, 41

Gallego, J., Zamorano, J., Aragón-Salamanca, A., & Rego, M. 1995, ApJ, 445, L1

García-Vargas, M. L., Bressan, A., & Díaz, A. I. 1995a, A&AS, 112, 13

García-Vargas, M. L., Bressan, A., & Díaz, A. I. 1995b, A&AS, 112, 35

García-Vargas, M. L., & Díaz, A. I. 1994, ApJS, 91, 553

García-Vargas, M. L. González-Delgado, R. M., Pérez, E., et al. 1997, ApJ, 478, 112

Giavalisco, M., Steidel, C. C., & Maccheto, F. D. 1996, ApJ, 470, 189

Girardi, L., Bressan, A., Chiosi, C., Bertelli, G., & Nasi, E. 1996, A&AS, 117, 113

Goldader, J. D., Joseph, R. D., Doyon, R., & Sanders, D. B. 1997, ApJ, 474, 104

González-Delgado, R. M., García-Vargas, M. L., Goldader, J., Leitherer, C., & Pasquali, A. 1999, ApJ, 513, 707

González-Delgado, R. M., Leitherer, C., Heckman, T., et al. 1998, ApJ, 495, 698

Greggio, L., Tosi, M., Clampin, M., et al. 1998, ApJ, 504, 725

Groenewegen, M., & De Jong, T. 1993, A&A, 267, 410

Heckman, T. M. 1991, in Massive Stars in Starbursts, ed. C. Leitherer, T. M. Heckman, & C. A. Norman (Cambridge University Press), 289

Keel, W. C. 1993, AJ, 106, 1771

Kennicutt, R. C. 1998, ARA&A, 36, 189

Kim, D. C., Veilleux, S., & Sanders, D. B. 1998, ApJ, 508, 627

Kurucz, R. L. 1992, Model Atmospheres for Population Synthesis, ed. B. Barbuy, & A. Renzini, The stellar populations of Galaxies, IAU Symp. 149 (Reidel, Dordrecht), 225

Lançon, A., & Rocca-Volmerange, B. 1996, New Astron. 1, 215

Leech, K. J., Penston, M. V., Terlevich, R., et al. 1989, MNRAS, 240, 349

Leitherer, C. 1998, in 38th Herstmonceux Conference, The Stellar Initial Mass function, ed. G. Gilmore, I. Parry, & S. Ryan (ASP, San Francisco), 61

Leitherer, C., Ferguson, H. C., Heckman, T. M., & Lowenthal, J. D. 1995, ApJ, 454, L19

Leitherer, C., & Heckman, T. M. 1995, ApJS, 96, 9

Leitherer, C., Robert, C., & Drissen, L. 1992, ApJ, 401, 596

Leitherer, C., Schaerer, D., Goldader, J. D., et al. 1999, ApJS, 123, 3

Leitherer, C., Vacca, W. D., Conti, P. S., et al. 1996, ApJ, 465, 717

Lejeune, T., Cuisinier, F., & Buser, R. 1997, A&AS, 125, 229

Lowenthal, J., Koo, D., Guzmán, R., et al. 1997, ApJ, 481, 673

Madau, P., Ferguson, H. C., Dickinson, M. E., et al. 1996, MNRAS, 283, 1388

Mas-Hesse, J. M., & Kunth, D. 1999, A&A, 349, 765

Mazzarella, J. M., & Balzano, V. 1986, ApJS, 85, 27

McCall, M. L., Rybski, P. M., & Shields, G. A. 1985, ApJS, 57, 1

McGaugh, S. 1991, ApJ, 380, 140

Olofsson, K. 1997, A&A, 321, 29

Rieke, G. H., Loken, K., Rieke, M. J., & Tamblyn, P. 1995, ApJ, 412, 99

Salpeter, E. E. 1955, ApJ, 121, 161

Schaerer, D. 1996, A&A, 309, 129

Shields, G. A. 1974, ApJ, 193, 335

Shields, G. A. 1978, ApJ, 219, 565

Shields, G. A. 1990, ARA&A, 28, 525

Shields, G. A., & Tinsley, B. M. 1976, ApJ, 203, 66

Stasińska, G. 1978, A&A, 66, 257

Stasińska, G. 1980, A&A, 84, 320

Stasińska, G., & Leitherer, C. 1996, ApJS, 107, 661

Stasińska, G., & Schaerer, D. 1997, A&A, 322, 615

Steidel, C. C., Giavalisco, M., Pettini, M., Dickinson, M., & Adelberger, K. L. 1996, ApJ, 462, L17

Storchi-Bergmann, T., Kinney, A. L., & Challis, P. 1995, ApJS, 98, 103

Terlevich, R. J. 1985, in Star Forming Dwarf Galaxies and Related Objects, ed. D. Kunth, T. X. Thuan, & J. T. Thanh Van (Éditions Frontières, Paris), 395

Terlevich, R., Melnick, J., Masegosa, J., Moles, M., & Copetti, M. V. F. 1991, A&AS, 91, 285

Vacca, W. D., Robert, C., Leitherer, C., & Conti, P. S. 1995, ApJ, 444, 647

Veilleux, S., Kim, D.-C., Sanders, D. B., Mazzarella, J. M., & Soifer, B. T. 1995, ApJS, 98, 171

Veilleux, S., & Osterbrock, D. E. 1987, ApJS, 63, 295